CCS Chemistry

RESEARCH ARTICLE

Received: July 11, 2024 | Accepted: Oct. 1, 2024 | Published: Oct. 30, 2024

Toward the Synthesis of Pentaheptite Substructure: The Cyclopenta[*ef*]heptalene to Phenanthrene Rearrangement

Chang Wang[1], Chenyu Hu[1], Weize Wang[1], Jun Yang[1] & Junzhi Liu[1,2,3]*

[1]*Department of Chemistry, HKU-CAS Joint Laboratory on New Materials and Shanghai-Hong Kong Joint Laboratory on Chemical Synthesis, The University of Hong Kong, Hong Kong SAR 999077,* [2]*State Key Laboratory of Synthetic Chemistry, The University of Hong Kong, Hong Kong SAR 999077,* [3]*Materials Innovation Institute for Life Sciences and Energy (MILES), HKU-SIRI, Shenzhen 518005*

**Corresponding author: juliu@hku.hk*

Cite this: *CCS Chem*. **2024**, Just Published. DOI: 10.31635/ccschem.024.202404765

Novel carbon allotropes have long been pursued in synthetic chemistry and materials science, and graphene has been the most well-investigated carbon nanostructure in the past decade. However, an analogous carbon pentaheptite with equal numbers of pentagons and heptagons has not yet been synthesized because designing and synthesizing nonhexagon motifs along two dimensions is challenging. During the synthesis of a pentaheptite substructure (or named nanopentaheptite, NPH), which contain four pentagon-heptagon pairs and one heptalene unit, unexpected cyclopenta[*ef*]heptalene-into-phenanthrene rearrangements were observed for the first time, yielding two novel compounds (NPH-R1 and NPH-R2). Experimental and theoretical results demonstrated that the NPH series exhibits narrower energy gaps than that of their hexagonal analog with similar size (e.g., hexa-peri-hexabenzocoronene, HBC). Our work reported herein, based on the azulene chemistry, provides new insights into the preparation of novel carbon allotrope pentaheptite nanostructures.

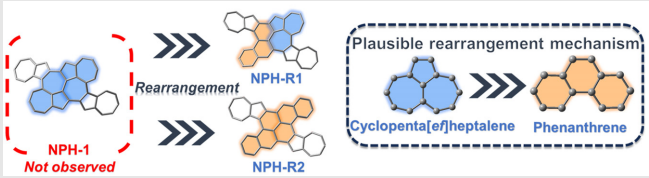

Keywords: **nanographene, pentaheptite, rearrangement, pentagons-heptagons, Pd-catalyzed**

Introduction

Carbon allotropes composed entirely of sp^2 hybridized carbons, including fullerenes (0D),[1] carbon nanotubes (1D),[2] and graphene (2D),[3] have been the most well-investigated class of carbon nanostructures over the past 30 years. Since it was first isolated in 2004, graphene has attracted much attention owing to its extremely high tensile strength, transparency, and conductivity, which makes it a promising material for next-generation electronic and photonic applications.[3,4] However, the application of graphene in field-effect transistor devices has been limited due to its zero bandgap.[5] Graphene molecules, which can be regarded as subunits of graphene, have been intensively investigated during the past two decades through bottom-up strategies; through these strategies, the size and edge topologies of graphene molecules can be atomically precisely controlled after their physical and chemical properties are

Citation: *CCS Chem.* **2024**, Just Published. DOI: 10.31635/ccschem.024.202404765
Link to VoR: https://doi.org/10.31635/ccschem.024.202404765

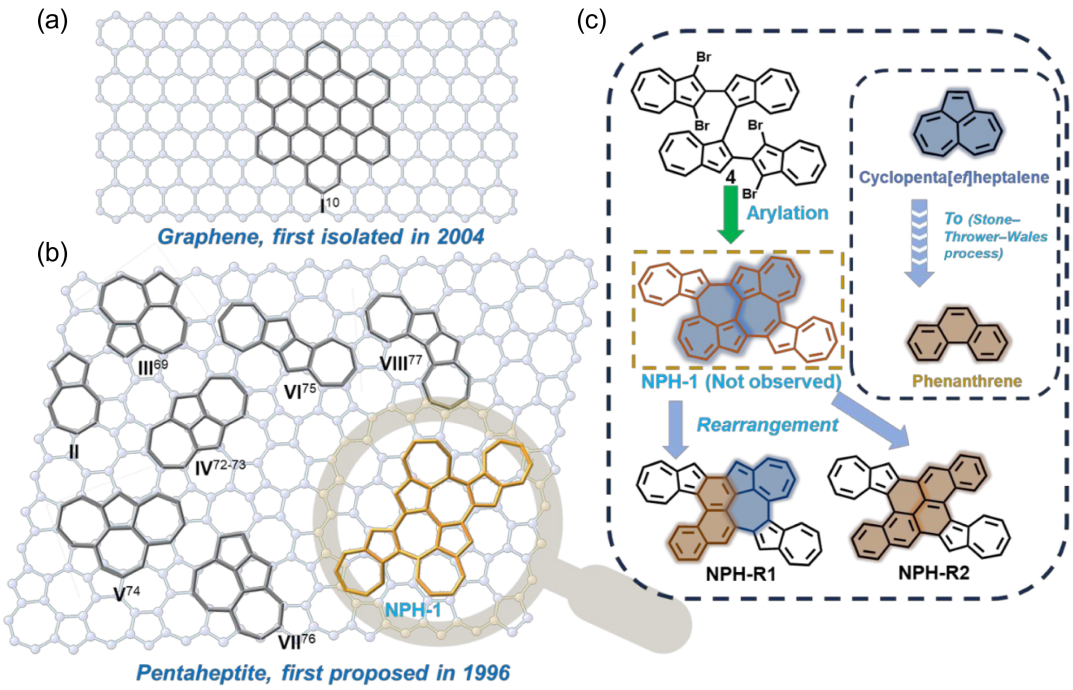

Figure 1 | *(a) The structures of graphene and **HBC**. (b) The structures of pentaheptite and several substructures of nanopentaheptites. (c) The rearrangement phenomenon during the arylation in this work.*

investigated.[5–13] For instance, hexa-peri-hexabenzocoronene (**I**, **HBC**, Figure 1a), which is a classic example of molecular graphene, has been widely studied as a molecular material in organic electronics.[10,14–17] Although these nanocarbons exhibiting a variety of properties have attracted extensive attention as functional molecules, the pursuit of new sp^2 carbon allotropes with novel structures exhibits great importance when considering the extraordinary electronic, optical, and magnetic properties of sp^2 carbon atoms.[18–39] Very recently, Gottfried and coworkers[40] reported a new sp^2 carbon allotrope containing four-, six-, and eight-membered rings, namely a biphenylene network, with metallic features rather than dielectric characteristics, showing enormous potential applications in carbon-based circuitry.

Although the development of carbon allotropes with different topological sp^2-carbon atoms has grown rapidly,[40–42] performing atomically precise synthesis of theoretically predicted nonbenzenoid carbon allotropes, such as pentaheptite,[43] T-graphene,[44,45] and R-haeckelite,[46] remains challenging. Among them, pentaheptite (Figure 1b), which was first proposed by Crespi in 1996, is a metallic isomer of graphene with equal numbers of pentagons and heptagons, and is metastable compared with graphene.[43] It has been predicted that with a dramatically increased density of states at the Fermi level, pentaheptite could yield a higher superconducting transition temperature (T_c).[43] In recent years, many efforts have been dedicated to designing and synthesizing carbon molecules with joined pentagonal and heptagonal rings (5–7 pairs), which have also attracted growing interest due to their unique physicochemical properties, for example, open-shell or abnormal anti-Kasha emission behavior.[47–67] However, an atomically precise synthesis of pentaheptite nanostructures remains elusive even though considerable effort has been expended to predict their physiochemical properties.

Azulene (**II**, Figure 1b), which can be regarded as a minimum unit of pentaheptite, has attracted much attention due to its extraordinary chemical and physical properties.[61–64,68] Azupyrene (**III**, Figure 1b), a well-known Stone-Wales defect in graphene, is the second-smallest unit of pentaheptite, and only sporadic investigations into its derivatives have been performed due to the difficulties in preparation.[50–55,69–71] Several similar size substructures of pentaheptite compared with azupyrene (**IV–VIII**, Figure 1b) have been achieved in the 20th century.[72–77] However, a larger sized unit of pentaheptite has not been achieved since Anderson et al.[69] reported the first synthesis and characterization of azupyrene in 1968. Further development in this domain is hindered because azulene exhibits high rearrangement activities (e.g., azulene into naphthalene) not only in solution[78] but also in solid form.[79–81] In this work, we have attempted to synthesize **NPH-1** in solution via an intramolecular arylation reaction of 1,1‴,3,3‴-tetrabromo-2,2′:1′,1″:2″,2‴-quaterazulene (Figure 1c). Interestingly, two novel rearrangement compounds, azuleno[2,1-c]azuleno[1′,2′:5,6]cyclohepta[3,4]azuleno[7,8,1-mna]phenanthrene (**NPH-R1**) and azuleno[1,2-f]benzo[c]cyclohepta[2,3]indeno

Citation: *CCS Chem.* **2024**, Just Published. DOI: 10.31635/ccschem.024.202404765
Link to VoR: https://doi.org/10.31635/ccschem.024.202404765

[4,5,6,7-pqr]tetraphene (**NPH-R2**), were obtained (Figure 1c), which involve the first discovery of cyclopenta[*ef*]heptalene to phenanthrene rearrangements (also could be defined as Stone-Thrower-Wales progress) in the experiment. The plausible rearrangement mechanism is proposed. From the ultraviolet–visible (UV-vis) absorption measurements, the optical energy gaps (E_g^{opt}) of **NPH-R1** and **NPH-R2** are estimated to be 2.03 and 2.37 eV, respectively. This result reveals that the **NPH** series with nonbenzenoid topologies has smaller energy gaps than that of benzenoid **HBC** (E_g^{opt} = 2.7 eV),[10] despite the similar size of the **NPH** series (C40) and **HBC** (C42). Nucleus-independent chemical shifts (NICS), the calculated anisotropy of the induced current density (ACID), and 2D iso-chemical shielding surface (ICSS) maps demonstrate that all peripheral azulene units in **NPH-R1** and **NPH-R2** display aromatic features (Figure 4 and Supporting Information Figure S18). Our work reported herein addresses the instability of five-seven membered rings and the challenges involved in the synthesis of a new novel 2D carbon allotrope pentaheptite.

Experimental Methods

Materials and methods

Dichloromethane (DCM), toluene (Tol), and tetrahydrofuran (THF) were dehydrated by solvent purification system (Inert) prior to use. All other reagents were purchased without any further purification. 2-Iodoazulene (**1**)[82] and 2-(1,3-dibromoazulen-2-yl)-4,4,5,5-tetramethyl-1,3,2-dioxaborolane (**2**)[83] were synthesized according to the reported literature. Further experimental details regarding the preparation of intermediates and target compounds are available in the Supporting Information Figures S1–S12.

Preparative thin layer chromatography (P02015, Analtech Brand Silica Gel GF TLC Plates 2000 μm 20 × 20 cm) was bought from Miles Scientific Company (Newark, DE, United States) and used as received. The UV–vis spectroscopy was conducted on an Agilent Cary 60. The fluorescent spectra were investigated using a Cary eclipse fluorescence spectrophotometer (Agilent Technologies, Santa Clara, CA, United States). Melting points were investigated with a Stuart Scientific SMP1 Analogue Melting Point Apparatus (Norrscope Ltd., Bicknacre, United Kingdom). High resolution mass spectra were obtained on a Bruker Q-Tof Maxis II mass spectrometer, a DFS high resolution magnetic sector mass spectrometer, and a Bruker Autoflex MALDI-TOF (Bruker Corporation, Billerica, MA, United States). Accurate masses from high-resolution mass spectra were reported for the molecular ion $[M]^+$, $[M+H]^+$, $[M+Na]^+$, or $[M+K]^+$. ^{1}H nuclear magnetic resonance (NMR) and ^{13}C NMR spectra were obtained on a Bruker 400 or 500 spectrometer (400/500 MHz for ^{1}H, 101/126 MHz for ^{13}C). Chemical shifts are reported as parts per million (ppm) with residual solvent signals as internal standard [DCM-d2 (CD_2Cl_2), δ = 5.32 ppm for ^{1}H NMR, δ = 54.00 ppm for ^{13}C NMR].[84] Data for ^{1}H NMR were presented as following: chemical shifts (δ, ppm), multiplicity (s = singlet, d = doublet, t = triplet, q = quartet, dd = doublet of doublets, tt = triplet of triplets, td = triplet of doublets, and m = multiplet), coupling constant (Hz), and integration.

Results and Discussion

Design and synthesis

To synthesize the target molecule, we chose azulene derivatives, the smallest units of pentaheptite, 2-iodoazulene (**1**)[82] and 2-(1,3-dibromoazulen-2-yl)-4,4,5,5-tetramethyl-1,3,2-dioxaborolane (**2**)[83] as the starting building blocks (Scheme 1). Through the Suzuki–Miyaura coupling reaction and followed by the Scholl reaction, key compound **4** was obtained as a dark green solid in approximately 18% yield. The structure of **4** was confirmed with NMR and high-resolution mass spectrometry. In the final step, an unexpected rearrangement of the cyclopenta[*ef*]heptalene unit into phenanthrene was observed during intramolecular arylation of **4**, affording **NPH-R1** and **NPH-R2** in 1% and 4% yields, respectively. The desired compound **NPH-1** was not observed.

The global optimum and low energy structure of **NPH-1** was 1.55 eV higher than that of **NPH-R1** based on the density functional theory (DFT) calculation at M062X/6-31g (d,p) level (Supporting Information Table S4). The structure of **NPH-R1** was 1.89 eV higher than that of **NPH-R2** at the same theoretical level (Supporting Information Table S4). It was therefore not surprising that **NPH-1** tended to rearrange into **NPH-R1** and **NPH-R2** during suitable reaction conditions. Plausible mechanisms were proposed for the cyclopenta[*ef*]heptalene to phenanthrene rearrangement, which involved the arenium ion pathway or Pd catalyst pathway (Supporting Information Figures S21 and S22). The arenium ion pathway was first considered assuming the rearrangement started from **NPH-1** (Supporting Information Figure S21). Through the protonation of **NPH-1** at position 1 of ring E, **NPH-2** could be generated with the energy barrier 56 kcal/mol. Due to the high energy barrier for protonation as well as the lack of acidic conditions during the reaction, the arenium ion rearrangement pathway seemed unreasonable. Another possible rearrangement mechanism might occur during the arylation, such as Pd-catalyzed rearrangement (Supporting Information Figure S22 and Table S5). To simplify the calculation, we ignored the effect of ligand and used **NPH-P1** as the start material. The critical rearrangement step involved the formation transition states of ***NPH-TS2***, ***NPH-TS3***, and/or ***NPH-TS5***. The intrinsic reaction

Citation: *CCS Chem.* **2024**, Just Published. DOI: 10.31635/ccschem.024.202404765
Link to VoR: https://doi.org/10.31635/ccschem.024.202404765

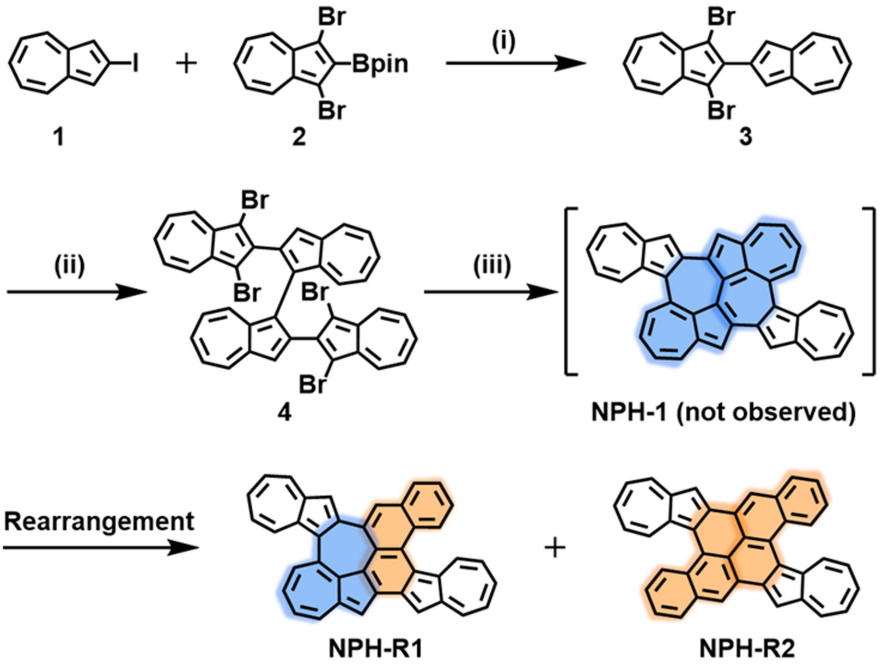

Scheme 1 | *Synthetic routes toward **NPH** series. (i) $Pd(PPh_3)_4$, K_2CO_3, THF/H_2O, 55 °C, 61%. (ii) $FeCl_3$, $MeNO_2$, DCM, –78 °C, 30%. (iii) $Pd(OAc)_2$, BINAP, K_2CO_3, toluene, 115 °C, 1% for **NPH-R1** and 4% for **NPH-R2**. Abbreviation: K_2CO_3, potassium carbonate; $Pd(PPh_3)_4$, tetrakis(triphenylphosphine)palladium(0); $FeCl_3$, Iron(III) chloride; $MeNO_2$, nitromethane; $Pd(OAc)_2$, palladium(II) acetate; BINAP, 2,2′-bis(diphenylphosphino)-1,1′-binaphthyl.*

coordinate paths showed that all the transition states of ***NPH-TSs*** could afford the desired starting materials and products (Supporting Information Figures S23–S25). Among them, the path of ***NPH-TS2*** broke the transannular bond (cyclopentadienyl and cycloheptatrienyl) in the azulene unit (highlight in blue in Supporting Information Figure S22) to form the naphthalene unit (**NPH-P5**) via 1,2 migration. The required activation energy was greater than the path of ***NPH-TS3***, which formed **NPH-P5** through the triangle ring in the azulene unit (highlight in blue in Supporting Information Figure S22). The first rearrangement therefore tended to form ***NPH-TS3*** through the triangle ring, giving the phenanthrene unit (**NPH-P6**). Similarly, the second rearrangement also preferred the formation of ***NPH-TS5*** via triangle unit to generate the naphthalene unit (**NPH-P9**), which thereafter dissociated Pd to give **NPH-R2**. It was worth noting that due to the rigid structure of **NPH-P8**, the activation energy for the formation of ***NPH-TS5*** was larger than that of ***NPH-TS3***; therefore, it was not surprising that **NPH-R1** could form in the reaction.

Single-crystal analyses of NPH-R1 and NPH-R2

Single crystals of **NPH-R1** and **NPH-R2** were obtained by slowly evaporating DCM/hexane (Hex) and DCM/methanol (MeOH) mixtures, respectively (Supporting Information Table S1). As shown in Figure 2a,b,d,e, **NPH-R1** and **NPH-R2** adopted butterfly-like conformations with double-helical structures, in which **NPH-R2** possessed double [5]helicenes with pentagon-heptagon pairs. The sums of torsional angles for the inner helicene rims (ϕ, highlighted in black) of **NPH-R1** were 48.5° for [4]helicene and 46.4° for [5]helicene, which were slightly smaller than those of **NPH-R2** (53.5° and 47.3° for each helical substructure) due to the negative curvature of the central heptagonal ring C in **NPH-R1**. The dihedral angles between the mean planes of the terminal rings (θ, highlighted in blue) in **NPH-R1** and **NPH-R2** were 42.0° (left) and 36.2° (right) as well as 42.4° (left) and 38.9° (right), respectively. These dihedral angles demonstrated that both **NPH-R1** and **NPH-R2** were not perfectly centrosymmetric, and **NPH-R2** was more twisted than **NPH-R1**. The alternating bond lengths of **NPH-R1** and **NPH-R2** indicated poor local aromaticity.[56,57] The bond lengths of the armchair edges between rings B, C, and G as well as rings D, H, and I in **NPH-R1** displayed double bond characteristics.

In the solid state, **NPH-R1** and **NPH-R2** were packed in a sandwich herringbone style (Figure 2g,h). However, the intermolecular interactions of **NPH-R1** and **NPH-R2** exhibited different behaviors. **NPH-R1** was packed via C–H···π interactions (black numbers) operating between

Citation: *CCS Chem.* **2024**, Just Published. DOI: 10.31635/ccschem.024.202404765
Link to VoR: https://doi.org/10.31635/ccschem.024.202404765

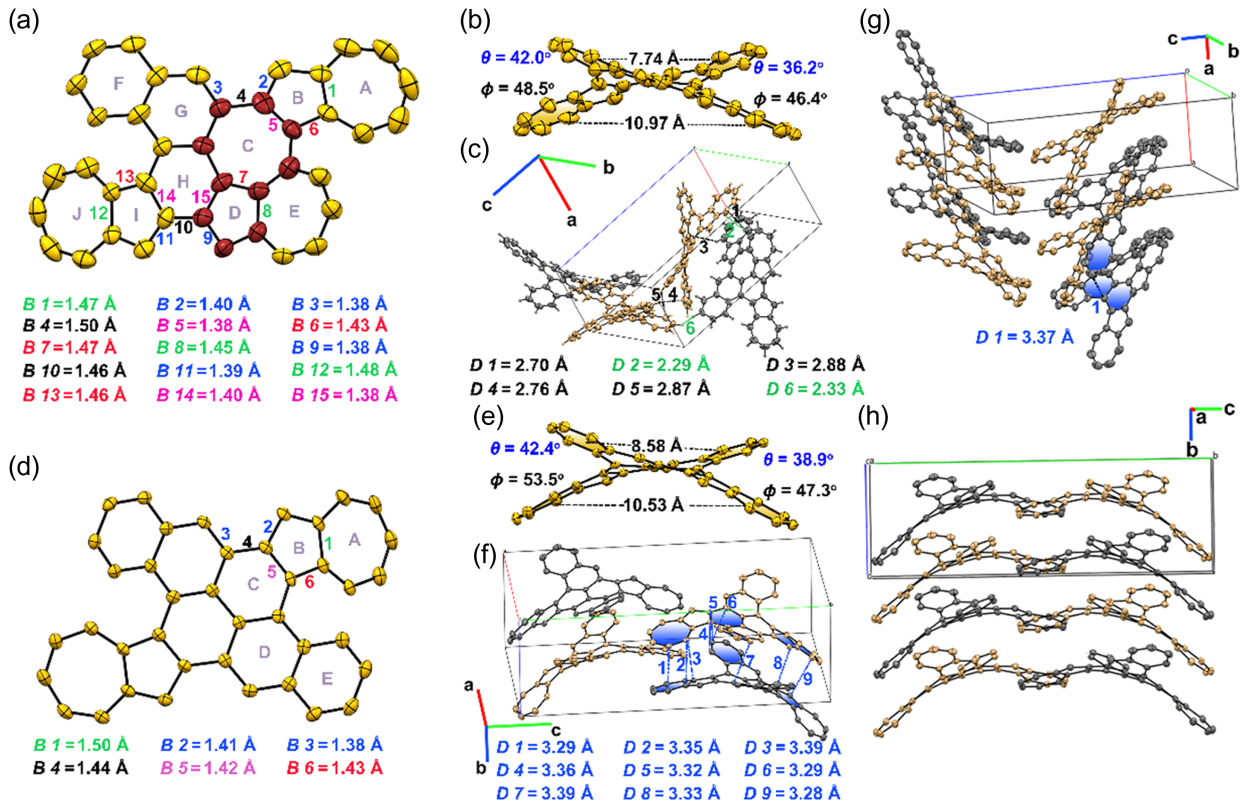

Figure 2 | *Single-crystal structures of* ***NPH-R1*** *and* ***NPH-R2****. (a) Front view of* ***NPH-R1****. (b) Side view of* ***NPH-R1****. (c) Packing structures of* ***NPH-R1*** *in the lattice unit. (d) Front view of* ***NPH-R2****. (e) Side view of* ***NPH-R2****. (f) Packing structures of* ***NPH-R2*** *in the lattice unit. (g) Packing style of* ***NPH-R1****. (h) Packing style of* ***NPH-R2****. For c, f, g, and h, orange:* MM*; gray:* PP*. Abbreviations:* B *= bond; and* D *= distance.*

adjacent dimers with carbon-to-hydrogen distances of 2.70–2.88 Å and van der Waals' forces (*VdW*, green numbers) with hydrogen-to-hydrogen distances of 2.29–2.33 Å (Figure 2c). The same configuration for **NPH-R1** (*PP*/*PP* and *MM*/*MM*) was arranged with an intermolecular π–π stacking distance of 3.37 Å between a heptagon and naphthalene (Figure 2g and Supporting Information Figure S13, highlighted in blue). In contrast, **NPH-R2** was mainly packed through π–π interactions with carbon-to-carbon distances of 3.28–3.39 Å (Figure 2f). The crystals of **NPH-R1** and **NPH-R2** were racemates of *PP*-/*MM*-**NPH-R1** and *PP*-/*MM*-**NPH-R2** because there were two pairs of enantiomers in one unit cell. The mesomeric structures of *PM*-**NPH-R1** and *PM*-**NPH-R2** were not observed in the solid state. The DFT calculations at the B3LYP-311G(d,p) level predicted that the activation energies of *PM*-**NPH-R1** to *MM*-**NPH-R1**, *MM*-**NPH-R1** to *MP*-**NPH-R1**, and *MP*-**NPH-R1** to *PP*-**NPH-R1** were 15.14, 12.87, and 14.76 kcal/mol, respectively (Supporting Information Figure S20a). The activation energies of *MP*-**NPH-R2** to *MM*-**NPH-R2** and *MM*-**NPH-R2** to *MP*-**NPH-R2** were calculated as 15.33 and 18.17 kcal/mol at the same level (Supporting Information Figure S20b). These theoretical results demonstrated that the conformational isomers of both **NPH-R1** and **NPH-R2** could flip freely at room temperature.

Optical and electrochemical properties of NPH-R1 and NPH-R2

The powders of **NPH-R1** and **NPH-R2** are both red-brown, while their similar hexagonal allotrope **tBu-HBC** is yellow, which could be attributed to the incorporation of azulene units into **NPH-R1** and **NPH-R2** and subsequent perturbation in their electronic structures. The solubilities of unsubstituted **NPH-R1** and **NPH-R2** were excellent in common organic solutions, including DCM, chloroform ($CHCl_3$), and THF. Interestingly, in dilute DCM solution, **NPH-R1** showed a red color, while **NPH-R2** displayed an orange color (Figure 3a). UV-vis absorption spectra of **NPH-R1** and **NPH-R2** were recorded in DCM (Figure 3a and Supporting Information Figure S14). Based on time-dependent density functional theory (TD-DFT) calculations at the B3LYP/6-311G(d,p) level, several very weak absorptions of **NPH-R1** were observed at 700–1000 nm corresponding to nearly forbidden S0→S1 (f = 0.0495) and forbidden S0→S2 (f = 0.0000) transitions (Supporting Information Table S2). Similarly, the weak tail

Citation: *CCS Chem.* **2024**, Just Published. DOI: 10.31635/ccschem.024.202404765
Link to VoR: https://doi.org/10.31635/ccschem.024.202404765

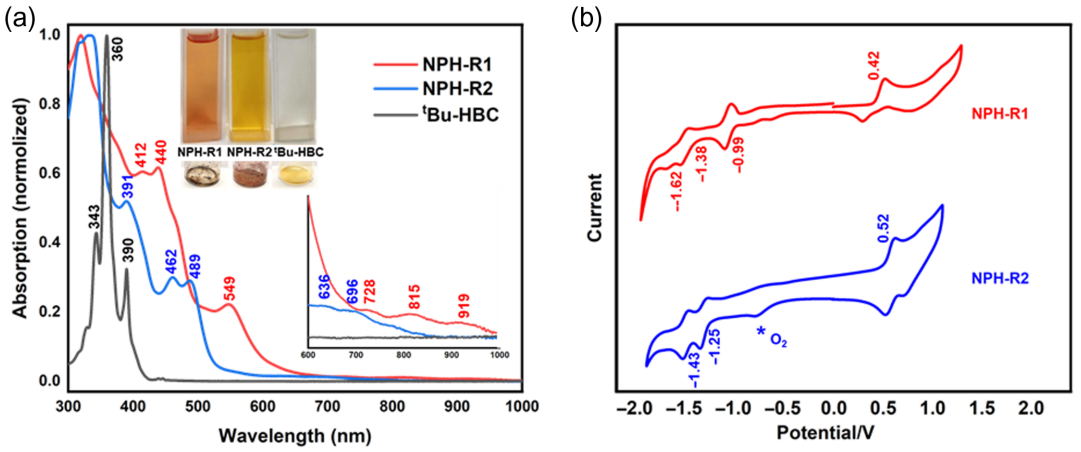

Figure 3 | *Spectroscopic and electrochemical characterization of **NPH-R1** and **NPH-R2**. (a) UV–vis spectra of **NPH-R1** (red), **NPH-R2** (blue), and **tBu-HBC** (black). (b) CVs of **NPH-R1** (red) and **NPH-R2** (blue). Scan rate: 50 mV/s. The brightness of the samples in solution and their solid states were increased by 10% and 30%, respectively.*

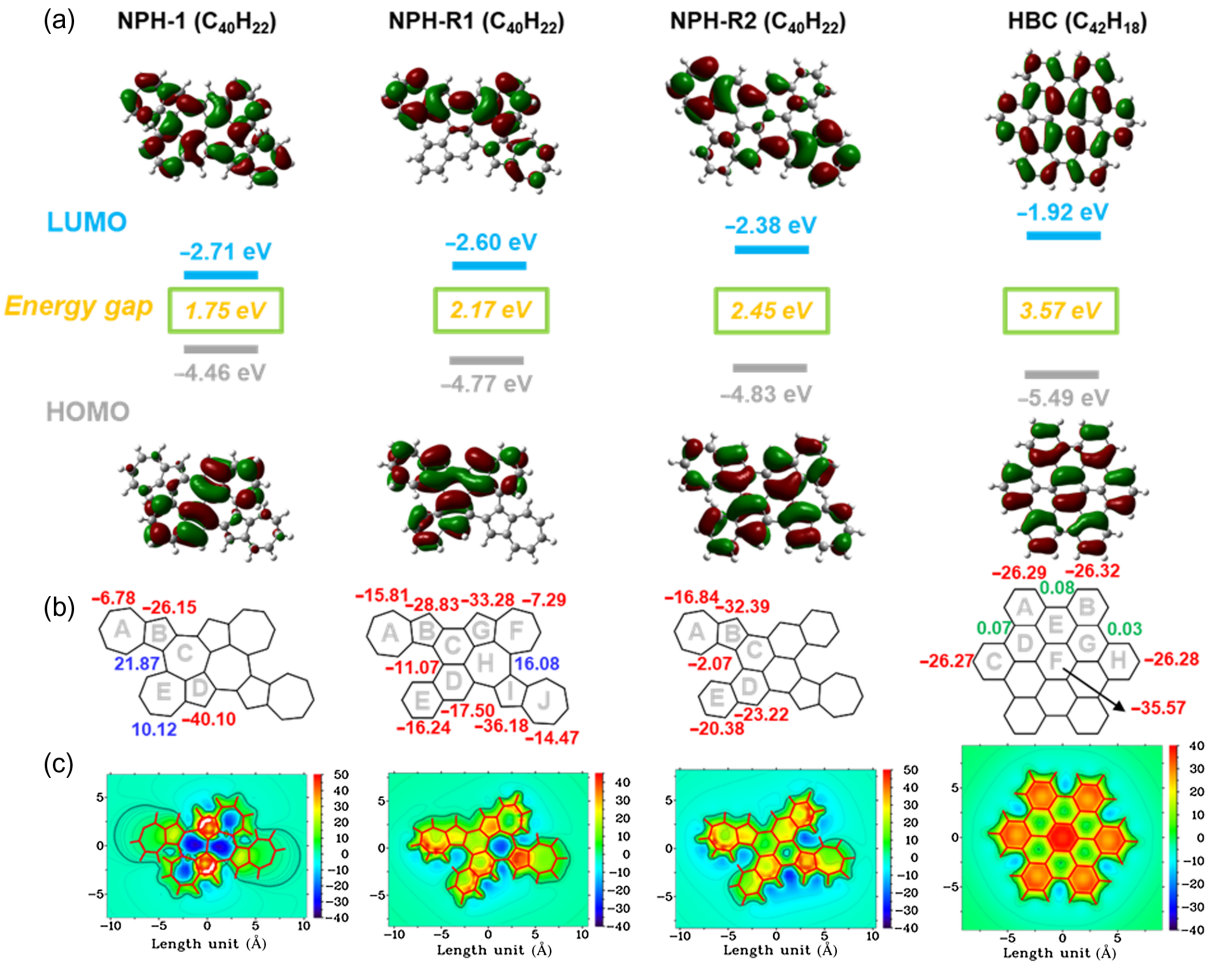

Figure 4 | *Theoretical calculations of the **NPH** series. (a) Molecular orbitals of the **NPH** series and **HBC**. (b) NICS(1)zz-avg calculation for the **NPH** series and **HBC**. (c) Calculated 2D ICSSzz maps for the **NPH** series and **HBC**.*

Citation: *CCS Chem.* **2024**, Just Published. DOI: 10.31635/ccschem.024.202404765
Link to VoR: https://doi.org/10.31635/ccschem.024.202404765

absorption appearing at 600-700 nm for **NPH-R2** was ascribed to the S0 to S1 transition due to a very weak oscillator strength (f = 0.0098) (Supporting Information Table S3). More significant redshifts were observed for both **NPH-R1** and **NPH-R2** than for **tBu-HBC** (approximately 465 nm). These bathochromic shifts indicated much smaller optical energy gaps (E_g^{opt}) for **NPH-R1** (2.03 eV) and **NPH-R2** (2.37 eV) compared with that of HBC (2.70 eV) on the basis of onset absorptions (λ_{onset}). Both **NPH-R1** and **NPH-R2** displayed weak anti-kasha fluorescence at around 500 nm (Supporting Information Figures S15 and S16).

A cyclic voltammogram (CV) determined spectrum for **NPH-R1** in DCM (Figure 3b, red line) showed that **NPH-R1** had one reversible oxidation wave at 0.42 V and two reversible reduction waves at –0.99 and –1.38 V, and an irreversible reduction potential of –1.62 V. Interestingly, the CV spectrum of **NPH-R2** in DCM (Figure 3b, blue line) exhibited one reversible oxidation potential at 0.52 V as well as two reversible reduction potentials at –1.25 and –1.43 V, while the monomeric helical azulene-embedded [5]helicene ([5]AzH) showed only one irreversible oxidation process and one reversible reduction process.[61] These results demonstrated that **NPH-R2** with double [5]AzH units exhibited better redox behavior than [5]AzH. Both **NPH-R1** and **NPH-R2** showed narrower reversible oxidation waves than **tBu-HBC** (1.06 V, Supporting Information Figure S17). The lowest unoccupied molecular orbital (LUMO)/highest occupied molecular orbital (HOMO) energy levels of **NPH-R1** and **NPH-R2** were calculated with the formula ($E_{LUMO/HOMO}$ = –(E_{red}^{onset}/E_{ox}^{onset} – E_{Fc} + 4.8) eV) to be –3.79/–5.20 eV and –3.53/–5.30 eV. Accordingly, the electrochemical energy gaps (E_g^{CV}) of **NPH-R1** and **NPH-R2** were calculated to be 1.41 and 1.77 eV, respectively.

Frontier molecular orbital and aromaticity analyse

TD-DFT calculations were carried out to study the electronic characteristics of these **NPH** series. Geometry optimization was performed at the B3LYP level with the 6-311G (d, p) basis set using the Gaussian16 package. As shown in Figure 4a, the **NPH** series exhibited a significantly smaller energy gap (from 1.75 to 2.45 eV) than that of **HBC** (3.57 eV). The LUMO distribution of **NPH**-series displayed a trend to disperse in nonalternant topologies (pentagons and heptagons). The local aromaticity of these NPH-series was investigated by the NICS calculated at GIAO-B3LYP/6-311+g (2d,p) level and ICSS maps at B3LYP/6-31+g (d) level. The peripheral pentagon-heptagon pairs in **NPH-R1** and **NPH-R2** showed aromatic features with negative value in NICSzz calculation (Figure 4b), which could also be supported by the magnetically shielded cavity in 2D and 3D (Figure 4c and Supporting Information Figure S19).[85-88] The peripheral heptagons adjacent to extra fused heptagons (rings C) in **NPH-1**, however, displayed antiaromatic properties. The aromaticity of extra fused heptagons in **NPH-1** and **NPH-R1** exhibited strong antiaromatic properties (26.87 for **NPH-1**, 16.08 for **NPH-R1**) as also corroborated by 2D ICSS (Supporting Information Figure S19) results. Accordingly, these four consecutive heptagons in **NPH-1** possess antiaromatic features, which could explain the instability of **NPH-1**, thus leading to the rearrangement. The remaining heptagons (ring A) in [5]helicenes of **NPH-R1** and **NPH-R2** exhibit aromatic characteristics, which is consistent with [5]AzH.[61] ACID (Supporting Information Figure S18) was calculated at CSGT-RB3LYP/6-311-g (d) level and further supported the local aromaticity of the **NPH**-series. The ring currents in **NPH**-series were closely matched with the results from NICS calculations.

Conclusion

In summary, we demonstrated the attempted synthesis of a substructure of pentaheptite. The designed nanopentaheptite **NPH-1** was not observed via the direct arylation reaction, interestingly, two nanocarbons (**NPH-R1** and **NPH-R2**) were obtained owing to the likely cyclopenta[*ef*]heptalene into phenanthrene rearrangements, which was first observed in the experiment. The unambiguous crystallographic characterizations of **NPH-R1** and **NPH-R2** showed that both molecules possess two helical structures, demonstrating butterfly-like geometries. All the **NPH** series (C_{40}) displayed narrow optical (2.03 eV for **NPH-R1** and 2.37 eV for **NPH-R2**) and electronic (1.41 eV for **NPH-R1** and 1.77 eV for **NPH-R2**) energy gaps compared with the similarly sized **HBC** (C_{42}) containing only six-membered rings. The possible rearrangement mechanism of cyclopenta[*ef*]heptalene into phenanthrene was proposed. Our work reported herein indicated that the synthesizing nanopentaheptite in solution is challenging due to unexpected rearrangements. Nevertheless, our group is investigating other strategies to prepare these novel pentahepite nanostructures.

Supporting Information

Supporting Information is available and includes experimental details and complete characterization of the newly prepared products, including NMR spectra and details of DFT calculations.

Conflict of Interest

The authors declare no competing interest.

Citation: *CCS Chem.* **2024**, Just Published. DOI: 10.31635/ccschem.024.202404765
Link to VoR: https://doi.org/10.31635/ccschem.024.202404765

Funding Information

This work was supported by the Hong Kong Research Grants Council (grant nos. 27301720, 17304021, and 17309023) and National Natural Science Foundation of China (grant no. 22122114). The work described in this paper was partially supported by a grant from the Co-funding Mechanism on Joint Laboratories with the Chinese Academy of Sciences (CAS) sponsored by the Research Grants Council of the Hong Kong Special Administrative Region, China and the CAS (Project No. JLFS/P-701/24 and Project No. JLFS/P-404/24).

Acknowledgments

J.L. is grateful for the funding from The University of Hong Kong (HKU) and Innovation and Technology Commission to the State Key Laboratories. We thank the University Grants Committee (UGC) funding administered by HKU for supporting the Time-of-Flight Mass Spectrometry Facilities under the Support for Interdisciplinary Research in Chemical Science. We acknowledge the computer cluster (HPC2021) of HKU for generous allocations of computer resources.

References

1. Kroto, H. W.; Heath, J. R.; O'Brien, S. C.; Curl, R. F.; Smalley, R. E. C_{60}: Buckminsterfullerene. *Nature* **1985**, *318*, 162–163.
2. Iijima, S. Helical Microtubules of Graphitic Carbon. *Nature* **1991**, *354*, 56–58.
3. Novoselov, K. S.; Geim, A. K.; Morozov, S. V.; Jiang, D.; Zhang, Y.; Dubonos, S. V.; Grigorieva, I. V.; Firsov, A. A. Electric Field Effect in Atomically Thin Carbon Films. *Science* **2004**, *306*, 666–669.
4. Novoselov, K.; Fal'ko, V.; Colombo, L.; Gellert, P. R.; Schwab, M. G.; Kim, K. A Roadmap for Graphene. *Nature* **2012**, *490*, 192–200.
5. Narita, A.; Wang, X. Y.; Feng, X.; Müllen, K. New Advances in Nanographene Chemistry. *Chem. Soc. Rev.* **2015**, *44*, 6616–6643.
6. Chen, L.; Mali, K. S.; Puniredd, S. R.; Baumgarten, M.; Parvez, K.; Pisula, W.; De Feyter, S.; Müllen, K. Assembly and Fiber Formation of a Gemini-Type Hexathienocoronene Amphiphile for Electrical Conduction. *J. Am. Chem. Soc.* **2013**, *135*, 13531–13537.
7. Wang, X. Y.; Narita, A.; Müllen, K. Precision Synthesis Versus Bulk-Scale Fabrication of Graphenes. *Nat. Rev. Chem.* **2018**, *2*, 0100.
8. Schuler, B.; Collazos, S.; Gross, L.; Meyer, G.; Pérez, D.; Guitián, E.; Peña, D. From Perylene to a 22-Ring Aromatic Hydrocarbon in One-Pot. *Angew. Chem. Int. Ed.* **2014**, *53*, 9004–9006.
9. Whalley, A. C.; Plunkett, K. N.; Gorodetsky, A. A.; Schenck, C. L.; Chiu, C. Y.; Steigerwald, M. L.; Nuckolls, C. Bending Contorted Hexabenzocoronene into a Bowl. *Chem. Sci.* **2011**, *2*, 132–135.
10. Böhme, T.; Simpson, C. D.; Müllen, K.; Rabe, J. P. Current-Voltage Characteristics of a Homologous Series of Polycyclic Aromatic Hydrocarbons. *Chem. Eur. J.* **2007**, *13*, 7349–7357.
11. Liu, J.; Feng, X. Synthetic Tailoring of Graphene Nanostructures with Zigzag-Edged Topologies: Progress and Perspectives. *Angew. Chem. Int. Ed.* **2020**, *59*, 23386–23401.
12. Biswas, K.; Soler, D.; Mishra, S.; Chen, Q.; Yao, X.; Sánchez-Grande, A.; Eimre, K.; Mutombo, P.; Martín-Fuentes, C.; Lauwaet, K.; Gallego, J. M.; Ruffieux, P.; Pignedoli, C. A.; Müllen, K.; Miranda, R.; Urgel, J. I.; Narita, A.; Fasel, R.; Jelínek, P.; E´cija, D. Steering Large Magnetic Exchange Coupling in Nanographenes Near the Closed-Shell to Open-Shell Transition. *J. Am. Chem. Soc.* **2023**, *145*, 2968–2974.
13. Mallada Faes, B. J.; Ondráček, M.; Lamanec, M.; Gallardo Caparrós, A. J.; Jiménez-Martín, A.; De La Torre Cerdeño, B.; Hobza, P.; Jelínek, P. Visualization of π-Hole in Molecules by Means of Kelvin Probe Force Microscopy. *Nat. Commun.* **2023**, *14*, 4954–4954.
14. Hill, J. P.; Jin, W.; Kosaka, A.; Fukushima, T.; Ichihara, H.; Shimomura, T.; Ito, K.; Hashizume, T.; Ishii, N.; Aida, T. Self-Assembled Hexa-Peri-Hexabenzocoronene Graphitic Nanotube. *Science* **2004**, *304*, 1481–1483.
15. Seyler, H., Purushothaman, B., Jones, D. J., Holmes, A. B. & Wong, W. W. H. Hexa-Peri-Hexabenzocoronene in Organic Electronics. *Pure Appl. Chem.* **2012**, *84*, 1047–1067.
16. Hassanpour, A.; Farhami, N.; Derakhshande, M.; Nezhad, P. D. K.; Ebadi, A.; Ebrahimiasl, S. Magnesium and Calcium Ion Batteries Based on the Hexa-Peri-Hexabenzocoronene Nanographene Anode Materials. *Inorg. Chem. Commun.* **2021**, *129*, 108656.
17. Jiménez, V. G.; David, A. H. G.; Cuerva, J. M.; Blanco, V.; Campaña, A. G. A Macrocycle Based on a Heptagon-Containing Hexa-Peri-Hexabenzocoronene. *Angew. Chem. Int. Ed.* **2020**, *59*, 15124–15128.
18. Tsefrikas, V. M.; Scott, L. T. Geodesic Polyarenes by Flash Vacuum Pyrolysis. *Chem. Rev.* **2006**, *106*, 4868–4884.
19. Yang, X.; Liu, D.; Miao, Q. Heptagon-Embedded Pentacene: Synthesis, Structures, and Thin-Film Transistors of Dibenzo[d,d']benzo[1,2-a:4,5-a']dicycloheptenes. *Angew. Chem. Int. Ed.* **2014**, *53*, 6786–6790.
20. Miao, Q. Heptagons in Aromatics: From Monocyclic to Polycyclic. *Chem. Rec.* **2015**, *15*, 1156–1159.
21. Cheung, K. Y.; Xu, X.; Miao, Q. Aromatic Saddles Containing Two Heptagons. *J. Am. Chem. Soc.* **2015**, *137*, 3910–3914.
22. Pun, S. H.; Miao, Q. Toward Negatively Curved Carbons. *Acc. Chem. Res.* **2018**, *51*, 1630–1642.
23. Pun, S. H.; Wang, Y.; Chu, M.; Chan, C. K.; Li, Y.; Liu, Z.; Miao, Q. Synthesis, Structures, and Properties of Heptabenzo[7]circulene and Octabenzo[8]circulene. *J. Am. Chem. Soc.* **2019**, *141*, 9680–9686.
24. Zhang, Y.; Pun, S. H.; Miao, Q. The Scholl Reaction as a Powerful Tool for Synthesis of Curved Polycyclic Aromatics. *Chem. Rev.* **2022**, *122*, 14554–14593.
25. Cheung, K. M.; Xiong, Y.; Pun, S. H.; Zhuo, X.; Gong, Q.; Zeng, X.; Su, S.; Miao, Q. Negatively Curved Molecular Nanocarbons Containing Multiple Heptagons are Enabled by the

Citation: *CCS Chem.* **2024**, Just Published. DOI: 10.31635/ccschem.024.202404765
Link to VoR: https://doi.org/10.31635/ccschem.024.202404765

Scholl Reactions of Macrocyclic Precursors. *Chem* **2023**, *9*, 2855–2868.
26. Amaya, T.; Hirao, T. Chemistry of Sumanene. *Chem. Rec.* **2015**, *15*, 310–321.
27. Márquez, I. R.; Fuentes, N.; Cruz, C. M.; Puente-Muñoz, V.; Sotorrios, L.; Marcos, M. L.; Choquesillo-Lazarte, D.; Biel, B.; Crovetto, L.; Gómez-Bengoa, E.; González, M. T.; Martin, R.; Cuerva, J. M.; Campaña, A. G. Versatile Synthesis and Enlargement of Functionalized Distorted Heptagon-Containing Nanographenes. *Chem. Sci.* **2017**, *8*, 1068–1074.
28. Márquez, I. R.; Castro-Fernández, S.; Millán, A.; Campaña, A. G. Synthesis of Distorted Nanographenes Containing Seven- and Eight-Membered Carbocycles. *Chem. Commun.* **2018**, *54*, 6705–6718.
29. Cruz, C. M.; Márquez, I. R.; Mariz, I. F. A.; Blanco, V.; Sánchez-Sánchez, C.; Sobrado, J. M.; Martín-Gago, J. A.; Cuerva, J. M.; Maçôas, E.; Campaña, A. G. Enantiopure Distorted Ribbon-Shaped Nanographene Combining Two-Photon Absorption-Based Upconversion and Circularly Polarized Luminescence. *Chem. Sci.* **2018**, *9*, 3917–3924.
30. Cruz, C. M.; Castro-Fernández, S.; Maçôas, E.; Cuerva, J. M.; Campaña, A. G. Undecabenzo[7]superhelicene: A Helical Nanographene Ribbon as a Circularly Polarized Luminescence Emitter. *Angew. Chem. Int. Ed.* **2018**, *57*, 14782–14786.
31. Cruz, C. M.; Márquez, I. R.; Castro-Fernández, S.; Cuerva, J. M.; Maçôas, E.; Campaña, A. G. A Triskelion-Shaped Saddle–Helix Hybrid Nanographene. *Angew. Chem. Int. Ed.* **2019**, *58*, 8068–8072.
32. Medel, M. A.; Tapia, R.; Blanco, V.; Miguel, D.; Morcillo, S. P.; Campaña, A. G. Octagon-Embedded Carbohelicene as a Chiral Motif for Circularly Polarized Luminescence Emission of Saddle-Helix Nanographenes. *Angew. Chem. Int. Ed.* **2021**, *60*, 6094–6100.
33. Medel, M. A.; Cruz, C. M.; Miguel, D.; Blanco, V.; Morcillo, S. P.; Campaña, A. G. Chiral Distorted Hexa-Peri-Hexabenzocoronenes Bearing a Nonagon-Embedded Carbohelicene. *Angew. Chem. Int. Ed.* **2021**, *60*, 22051–22056.
34. Mora-Fuentes, J. P.; Codesal, M. D.; Reale, M.; Cruz, C. M.; Jiménez, V. G.; Sciortino, A.; Cannas, M.; Messina, F.; Blanco, V.; Campaña, A. G. Heptagon-Containing Nanographene Embedded into [10]Cycloparaphenylene. *Angew. Chem. Int. Ed.* **2023**, *62*, e202301356.
35. Kawasumi, K.; Zhang, Q.; Segawa, Y.; Scott, L. T.; Itami, K. A Grossly Warped Nanographene and the Consequences of Multiple Odd-Membered-Ring Defects. *Nat. Chem.* **2013**, *5*, 739–744.
36. Matsubara, S.; Koga, Y.; Segawa, Y.; Murakami, K.; Itami, K. Creation of Negatively Curved Polyaromatics Enabled by Annulative Coupling that Forms an Eight-Membered Ring. *Nat. Catal.* **2020**, *3*, 710–718.
37. Chaolumen;Stepek, I. A.; Yamada, K. E.; Ito, H.; Itami, K. Construction of Heptagon-Containing Molecular Nanocarbons. *Angew. Chem. Int. Ed.* **2021**, *60*, 23508–23532.
38. Stepek, I. A.; Nagase, M.; Yagi, A.; Itami, K. New Paradigms in Molecular Nanocarbon Science. *Tetrahedron* **2022**, *123*, 132907.
39. González Miera, G.; Matsubara, S.; Kono, H.; Murakami, K.; Itami, K. Synthesis of Octagon-Containing Molecular Nanocarbons. *Chem. Sci.* **2022**, *13*, 1848–1868.
40. Fan, Q.; Yan, L.; Tripp, M. W.; Krejčí, O.; Dimosthenous, S.; Kachel, S. R.; Chen, M.; Foster, A. S.; Koert, U.; Liljeroth, P.; Gottfried, J. M. Biphenylene Network: A Nonbenzenoid Carbon Allotrope. *Science* **2021**, *372*, 852–856.
41. Fan, Q.; Martin-Jimenez, D.; Ebeling, D.; Krug, C. K.; Brechmann, L.; Kohlmeyer, C.; Hilt, G.; Hieringer, W.; Schirmeisen, A.; Gottfried, J. M. Nanoribbons with Nonalternant Topology from Fusion of Polyazulene: Carbon Allotropes Beyond Graphene. *J. Am. Chem. Soc.* **2019**, *141*, 17713–17720.
42. Hou, L.; Cui, X.; Guan, B.; Wang, S.; Li, R.; Liu, Y.; Zhu, D.; Zheng, J. Synthesis of a Monolayer Fullerene Network. *Nature* **2022**, *606*, 507–510.
43. Crespi, V. H.; Benedict, L. X.; Cohen, M. L.; Louie, S. G. Prediction of a Pure-Carbon Planar Covalent Metal. *Phys. Rev. B* **1996**, *53*, R13303–R13305.
44. Liu, Y.; Wang, G.; Huang, Q.; Guo, L; Chen, X. Structural and Electronic Properties of T Graphene: A Two-Dimensional Carbon Allotrope with Tetrarings. *Phys. Rev. Lett.* **2012**, *108*, 225505.
45. Xu, L.-C.; Wang, R.-Z.; Miao, M.-S.; Wei, X.-L.; Chen, Y.-P.; Yan, H.; Lau, W.-M.; Liu, L.-M.; Ma, Y.-M. Two Dimensional Dirac Carbon Allotropes from Graphene. *Nanoscale* **2014**, *6*, 1113–1118.
46. Terrones, H.; Terrones, M.; Hernández, E.; Grobert, N.; Charlier, J. C.; Ajayan, P. M. New Metallic Allotropes of Planar and Tubular Carbon. *Phys. Rev. Lett.* **2000**, *84*, 1716–1719.
47. Wang, M.-W.; Fan, W.; Li, X.; Liu, Y.; Li, Z.; Jiang, W.; Wu, J.; Wang, Z. Molecular Carbons: How Far Can We Go? *ACS Nano* **2023**, *17*, 20734–20752.
48. Zou, Y.; Han, Y.; Wu, S.; Hou, X.; Chow, C. H. E.; Wu, J. Scholl Reaction of Perylene-Based Polyphenylene Precursors Under Different Conditions: Formation of Hexagon or Octagon? *Angew. Chem. Int. Ed.* **2021**, *60*, 17654–17663.
49. Zou, Y.; Zeng, W.; Gopalakrishna, T. Y.; Han, Y.; Jiang, Q.; Wu, J. Dicyclopenta[4,3,2,1-ghi:4′,3′,2′,1′-pqr]perylene: A Bowl-Shaped Fragment of Fullerene C_{70} with Global Antiaromaticity. *J. Am. Chem. Soc.* **2019**, *141*, 7266–7270.
50. Konishi, A.; Horii, K.; Shiomi, D.; Sato, K.; Takui, T.; Yasuda, M. Open-Shell and Antiaromatic Character Induced by the Highly Symmetric Geometry of the Planarh Structure: Synthesis and Characterization of a Nonalternant Isomer of Bisanthene. *J. Am. Chem. Soc.* **2019**, *141*, 10165–10170.
51. Konishi, A.; Yasuda, M. Breathing New Life into Nonalternant Hydrocarbon Chemistry: Syntheses and Properties of Polycyclic Hydrocarbons Containing Azulene, Pentalene, and Heptalene Frameworks. *Chem. Lett.* **2021**, *50*, 195–212.
52. Horii, K.; Kishi, R.; Nakano, M.; Shiomi, D.; Sato, K.; Takui, T.; Konishi, A.; Yasuda, M. Bis-periazulene (Cyclohepta[def]fluorene) as a Nonalternant Isomer of Pyrene: Synthesis and Characterization of Its Triaryl Derivatives. *J. Am. Chem. Soc.* **2022**, *144*, 3370–3375.
53. Konishi, A.; Horii, K.; Hirose, M.; Yasuda, M. Bis-periazulene: Remaining Non-Alternant Isomer of Pyrene. *Pure Appl. Chem.* **2023**, *95*, 353–362.

Citation: *CCS Chem.* **2024**, Just Published. DOI: 10.31635/ccschem.024.202404765
Link to VoR: https://doi.org/10.31635/ccschem.024.202404765

54. Konishi, A.; Horii, K.; Yasuda, M. The Road to Bis-peri-azulene (Cyclohepta[def]fluorene): Realizing One of the Long-Standing Dreams in Nonalternant Hydrocarbons. *J. Phys. Org. Chem.* **2023**, *36*, e4495.
55. Mizuno, Y.; Nogata, A.; Suzuki, M.; Nakayama, K. I.; Hisaki, I.; Kishi, R.; Konishi, A.; Yasuda, M. Synthesis and Characterization of Dibenzothieno[a,f]pentalenes Enabling Large Antiaromaticity and Moderate Open-Shell Character through a Small Energy Barrier for Bond-Shift Valence Tautomerization. *J. Am. Chem. Soc.* **2023**, *145*, 20595–20609.
56. Liu, J.; Mishra, S.; Pignedoli, C. A.; Passerone, D.; Urgel, J. I.; Fabrizio, A.; Lohr, T. G.; Ma, J.; Komber, H.; Baumgarten, M.; Corminboeuf, C.; Berger, R.; Ruffieux, P.; Müllen, K.; Fasel, R.; Feng, X. Open-Shell Nonbenzenoid Nanographenes Containing Two Pairs of Pentagonal and Heptagonal Rings. *J. Am. Chem. Soc.* **2019**, *141*, 12011–12020.
57. Fei, Y.; Liu, J. Synthesis of Defective Nanographenes Containing Joined Pentagons and Heptagons. *Adv. Sci.* **2022**, *9*, e2201000.
58. Zhang, X.-S.; Huang, Y.-Y.; Zhang, J.; Meng, W.; Peng, Q.; Kong, R.; Xiao, Z.; Liu, J.; Huang, M.; Yi, Y.; Chen, L.; Fan, Q.; Lin, G.; Liu, Z.; Zhang, G.; Jiang, L.; Zhang, D. Dicyclohepta[ijkl,uvwx]rubicene with Two Pentagons and Two Heptagons as a Stable and Planar Non-benzenoid Nanographene. *Angew. Chem. Int. Ed.* **2020**, *59*, 3529–3533.
59. Qin, L.; Huang, Y.; Wu, B.; Pan, J.; Yang, J.; Zhang, J.; Han, G.; Yang, S.; Chen, L.; Yin, Z.; Shu, Y; Jiang, L.; Yi, Y; Peng, Q.; Zhou, X.; Li, L.; Zhang, G.; Zhang, X.; Wu, K.; Zhang, D. Diazulenorubicene as a Non-benzenoid Isomer of peri-Tetracene with Two Sets of 5/7/5 Membered Rings Showing Good Semiconducting Property. *Angew. Chem. Int. Ed.* **2023**, *62*, e202304632.
60. Huang, Y.-Y.; Wu, B.; Shi, D.; Liu, D.; Meng, W.; Ma, J.; Qin, L.; Li, C.; Zhang, G.; Zhang, X.-S.; Zhang, D. A Heptacene Analogue Entailing a Quinoidal Benzodi[7]annulene (7/6/7 Ring) Core with a Tunable Configuration and Multiple Redox Properties. *Angew. Chem. Int. Ed.* **2023**, *62*, e202300990.
61. Duan, C.; Zhang, J.; Xiang, J.; Yang, X.; Gao, X. Azulene-Embedded [n]helicenes (n=5, 6 and 7). *Angew. Chem. Int. Ed.* **2022**, *61*, e202201494.
62. Yang, X.; Hoffmann, M.; Rominger, F.; Kirschbaum, T.; Dreuw, A.; Mastalerz, M. Functionalized Contorted Polycyclic Aromatic Hydrocarbons by a One-Step Cyclopentannulation and Regioselective Triflyloxylation. *Angew. Chem. Int. Ed.* **2019**, *58*, 10650–10654.
63. Yang, X.; Rominger, F.; Mastalerz, M. Contorted Polycyclic Aromatic Hydrocarbons with Two Embedded Azulene Units. *Angew. Chem. Int. Ed.* **2019**, *58*, 17577–17582.
64. Kirschbaum, T.; Rominger, F.; Mastalerz, M. A Chiral Polycyclic Aromatic Hydrocarbon Monkey Saddle. *Angew. Chem. Int. Ed.* **2020**, *59*, 270–274.
65. Fernández-García, J. M.; Evans, P. J.; Medina Rivero, S.; Fernández, I.; García-Fresnadillo, D.; Perles, J.; Casado, J.; Martín, N. π-Extended Corannulene-Based Nanographenes: Selective Formation of Negative Curvature. *J. Am. Chem. Soc.* **2018**, *140*, 17188–17196.
66. Urieta-Mora, J.; Krug, M.; Alex, W.; Perles, J.; Fernández, I.; Molina-Ontoria, A.; Guldi, D. M.; Martín, N. Homo and Hetero Molecular 3D Nanographenes Employing a Cyclooctatetraene Scaffold. *J. Am. Chem. Soc.* **2020**, *142*, 4162–4172.
67. Pérez-Elvira, E.; Barragán, A.; Chen, Q.; Soler-Polo, D.; Sánchez-Grande, A.; Vicent, D. J.; Lauwaet, K.; Santos, J.; Mutombo, P.; Mendieta-Moreno, J. I.; De La Torre Cerdeño, B.; Gallego, J. M.; Miranda, R.; Martín, N.; Jelínek, P.; Urgel, D.; Écija, J. I. Generating Antiaromaticity in Polycyclic Conjugated Hydrocarbons by Thermally Selective Skeletal Rearrangements at Interfaces. *Nat. Synth.* **2023**, *1*, 1005–1016.
68. Ong, A.; Tao, T.; Jiang, Q.; Han, Y.; Ou, Y.; Huang, K. W.; Chi, C. Azulene-Fused Acenes. *Angew. Chem. Int. Ed.* **2022**, *61*, e202209286.
69. Anderson, A. G.; MacDonald, A. A.; Montana, A. F. Dicyclopenta[ef,k1]heptalene (azupyrene). *J. Am. Chem. Soc.* **1968**, *90*, 2993–2994.
70. Klein, B. P.; Ruppenthal, L.; Hall, S. J.; Sattler, L. E.; Weber, S. M.; Herritsch, J.; Jaegermann, A.; Maurer, R. J.; Hilt, G.; Gottfried, M. Topology Effects in Molecular Organic Electronic Materials: Pyrene and Azupyrene. *ChemPhysChem* **2021**, *22*, 1065–1073.
71. Klein, B. P.; Ihle, A.; Kachel, S. R.; Ruppenthal, L.; Hall, S. J.; Sattler, L.; Weber, S. M.; Herritsch, J.; Jaegermann, A.; Ebeling, D.; Maurer, R. J.; Hilt, G.; Tonner-Zech, R.; Schirmeisen, A.; Gottfried, J. M. Topological Stone-Wales Defects Enhance Bonding and Electronic Coupling at the Graphene/Metal Interface. *ACS Nano* **2022**, *16*, 11979–11987.
72. Reel, H.; Vogel, E. Dicyclohepta[cd, gh]pentalene-A New Pyrene Isomer. *Angew. Chem. Int. Ed.* **1972**, *11*, 1013–1014.
73. Mathey, P.; Lirette, F.; Fernández, I.; Renn, L.; Weitz, R. T.; Morin, J. F. Annulated Azuleno[2, 1, 8-ija]azulenes: Synthesis and Properties. *Angew. Chem. Int. Ed.* **2023**, *62*, e202216281.
74. Hafner, K.; Hafner-Schneider, G.; Bauer, F. Azuleno [8,8a,1, 2-def]heptalene. *Angew. Chem. Int. Ed.* **1968**, *7*, 10.
75. Toda, T.; Shimazaki, N.; Mukai, T.; Kabuto, C. Synthesis and Physical Properties of 6, 12-diarylazuleno[1, 2-b]azulenes. *Tetrahedron Lett.* **1980**, *21*, 4001–4004.
76. Hafner, K.; Fleischer, R.; Fritz, K. Pentaleno[2, 1, 6-def] heptalene–A Non-benzenoid Isomer of Pyrene. *Angew. Chem. Int. Ed.* **1965**, *4*, 69–70.
77. Nitta, M.; Nishimura, K.; Iino, Y. Synthesis and Structural Studies of Novel Azuleno[1, 2-a]azulene and Its Derivatives. *Tetrahedron Lett.* **1993**, *34*, 2151–2160.
78. Das, S.; Wu, J. Toward Singlet-Triplet Bistable Nonalternant Kekule Hydrocarbons: Azulene-to-Naphthalene Rearrangement. *Org. Lett.* **2015**, *17*, 5854–5857.
79. Shiotari, A.; Nakae, T.; Iwata, K.; Mori, S.; Okujima, T.; Uno, H.; Sakaguchi, H.; Sugimoto, Y. Strain-Induced Skeletal Rearrangement of a Polycyclic Aromatic Hydrocarbon on a Copper Surface. *Nat. Commun.* **2017**, *8*, 16089.
80. Anderson, A. G.; Daugs, E. D.; Kao, L. G.; Wang, J. F. Dicyclopenta[ef,kl]heptalene (Azupyrene) Chemistry. Jutz Synthesis Byproducts. Synthesis and Thermal Isomerization of 1-Methylazupyrene. *J. Org. Chem.* **1986**, *51*, 2961–2965.
81. Mirzaei, M. S.; Taherpour, A. A.; Wentrup, C. Thermal Rearrangement of Azulenes to Naphthalenes: A Deeper Insight into the Mechanisms. *J. Org. Chem.* **2022**, *87*, 3296–3310.

Citation: *CCS Chem.* **2024**, Just Published. DOI: 10.31635/ccschem.024.202404765
Link to VoR: https://doi.org/10.31635/ccschem.024.202404765

82. Narita, M.; Murafuji, T.; Yamashita, S.; Fujinaga, M.; Hiyama, K.; Oka, Y.; Tani, F.; Kamijo, S.; Ishiguro, K. Synthesis of 2-Iodoazulenes by the Iododeboronation of Azulen-2-ylboronic Acid Pinacol Esters with Copper(I) Iodide. *J. Org. Chem.* **2018**, *83*, 1298–1303.
83. Lvov, A. G.; Bredihhin, A.; Peet, J.; Yadykov, A. V.; Dmitrienko, A. O.; Shirinian, V. Z. 1,2-Bis- and 1,2,3-Tris(2,5-dimethylthiophen-3-yl)azulenes: Synthesis, Structure and Properties. *Dyes Pigm.* **2020**, *172*, 107843.
84. Budavari, S.; O'Neil, M.J.; Smith, A.; Heckelman, P. E. *The Merck Index, an Encyclopedia of Chemicals, Drugs, and Biologicals*, 11th ed.; Merck Co., Inc.: Rahway, NJ, **1989**.
85. Klod, S.; Kleinpeter, E. Ab Initio Calculation of the Anisotropy Effect of Multiple Bonds and the Ring Current Effect of Arenes—Application in Conformational and Configurational Analysis. *J. Chem. Soc., Perkin Trans. 2* **2001**, *2*, 1893–1898.
86. Lu, T.; Chen, F. M. Multiwfn: A Multifunctional Wavefunction Analyzer. *J. Comput. Chem.* **2012**, *33*, 580.
87. Liu, Z.; Lu, T.; Chen, Q. An Sp-Hybridized All-Carboatomic Ring, Cyclo[18]carbon: Bonding Character, Electron Delocalization, and Aromaticity. *Carbon* **2020**, *165*, 468–475.
88. Humphrey, W.; Dalke, A.; Schulten, K. VMD: Visual Molecular Dynamics. *J. Mol. Graphics* **1996**, *14*, 33.

Citation: *CCS Chem.* **2024**, Just Published. DOI: 10.31635/ccschem.024.202404765
Link to VoR: https://doi.org/10.31635/ccschem.024.202404765